Journal of Molecular Spectroscopy **205,** 20–27 (2001)
doi:10.1006/jmsp.2000.8232, available online at http://www.idealibrary.com on IDEAL®

Collisional-Broadened and Dicke-Narrowed Lineshapes of $H_2{}^{16}O$ and $H_2{}^{18}O$ Transitions at 1.39 μm

L. Moretti,* A. Sasso,* L. Gianfrani,† and R. Ciurylo‡

*Dipartimento di Scienze Fisiche, Università di Napoli "Federico II" and INFM, Via Cinthia, Complesso Universitario Monte S. Angelo, 80125 Naples, Italy; †Dipartimento di Scienze Ambientali, Seconda Università di Napoli and INFM, Via Vivaldi, 81100 Caserta, Italy; and ‡Institute of Physics, Nicholas Copernicus University, Grudziadzka 5/7, PL-87-100 Torun, Poland

E-mail: sasso@na.infn.it

Received May 18, 2000; in revised form September 18, 2000

We present results of a study on the self-broadening and broadening by nitrogen and oxygen of $H_2{}^{16}O$ and $H_2{}^{18}O$ lines in the 1.39-μm wavelength region using a distributed feedback semiconductor diode laser. To estimate the broadening coefficients, the absorption lineshapes were analyzed using the ordinary Voigt profile which provided good fits for most of the investigated lines. The broadening coefficients were found to be larger for nitrogen used as a perturber than for oxygen. This agrees with the fact that the quadrupole moment of N_2 is larger than that of O_2. Nevertheless, for lines involving high-rotational quantum number J, relatively smaller broadening coefficients were found and deviations of the measured profiles from the standard Voigt profile were observed. These deviations were ascribed as caused by Dicke-narrowing effect. Corresponding to this effect, collisional-broadening and narrowing coefficients were determined using the Nelkin–Ghatak profile which is suitable for the "hard"-collision model. The optical diffusion coefficients of the water in both nitrogen and oxygen gases were determined from the measurements of the collisional-narrowing coefficients.

1. INTRODUCTION

The shape of absorbed or emitted molecular (or atomic) lines is usually modeled as a combination of Doppler broadening and collisional broadening. The former arises from the thermal motion of emitters (or absorbers), and the latter arises from perturbation of their internal states induced by collisions with perturbing particles (perturber). If these broadening mechanisms are considered to act independently, then the spectral lineshape is well represented by the familiar Voigt profile (VP).

However, this simplified model fails, for instance, in presence of collisions that induce velocity changes which produce a lineshape narrower than the profile obtained from ordinary Doppler-broadening theory (Dicke narrowing) (*1*). The lineshape of the generalized Doppler broadening depends on the assumed model describing velocity-changing collisions. Mainly, two models are used to describe velocity-changing collisions: the so-called "soft" and "hard" collision, depending on the mass ratio between absorber and perturber. In the soft- and hard-collision approximations, the Doppler-broadened lineshape is described by the Galatry profile (GP) (*2*) and the Nelkin–Ghatak profile (NGP) (*3*), respectively. Doppler- and collisional-broadened and shifted lineshapes were carefully discussed by Rautian and Sobelman (*4*), taking into account Dicke narrowing in both soft- and hard-collision approaches as well as correlation between velocity-changing and dephasing collisions.

Other important features which should be taken into account are the dependence of some collisional parameters such as the Lorentzian width and shift on the emitter speed, as was first indicated by Berman (*5*) and other authors (*6–11*). If speed-dependence of the collisional width and shift must be taken into account and Dicke narrowing can be neglected, the lineshape should be described by the speed-dependent Voigt profile (SDVP) given by Berman (*5*).

Duggan *et al.* (*12*) have shown that in some cases both the Dicke-narrowing and speed-dependent effects should be considered. The speed-dependent Galatry profile (SDGP) and speed-dependent Nelkin–Ghatak profile (SDNGP) have been given in Refs. (*13*) and (*14*), respectively. In recent years many experimental and theoretical investigations have been done in this field and a review of these results can be found in Refs. (*15–21*).

In this paper we have performed an experimental investigation of collision-broadened lineshape for several rovibrational transitions of water vapor with high resolution and accuracy. These lines belong to the combination band $\nu_1 + \nu_3$ and to the first overtone band $2\nu_1$ within the spectral range between 7181 and 7194 cm^{-1}. Pure absorption spectroscopy was performed using as a laser source a distributed feedback diode laser. We determined the pressure-broadening coefficients for four lines of $H_2{}^{16}O$ and for three lines of its isotopic species $H_2{}^{18}O$ using as perturber both N_2 and O_2. Moreover, for three of the investigated lines, the self-broadening coefficients were measured. These spectroscopic parameters are important not only for the

0022-2852/01 $35.00

collisional physics itself but are precious also for atmospheric lidar applications or for gas-trace detection by using high-sensitivity spectroscopic techniques.

The lineshape of most of the lines investigated in this work were well fitted by using the standard VP, while for lines involving high-rotational quantum numbers appreciable deviations were observed. These deviations were ascribed to the Dicke narrowing caused by velocity-changing collisions. Similar observations were also made by Eng *et al.* (*22*) for water vapor lines, broadened by argon and xenon, in the 5-μm wavelength region, and by Grossmann and Browell (*23, 24*), which investigated self-, N_2-, O_2-, Ar-, and air-broadening for lines belonging to the overtone vibrational band 4ν in the 720-nm wavelength l range. More recently, Avetison *et al.* (*25*) have evidenced Dicke narrowing in water vapor lines at 1.8 μm by using as a fit profile a Voigt convolution with a floating Gaussian component.

In the present work the spectra affected by Dicke narrowing were successfully fitted using the Nelkin–Ghatak hard-collision profile. In our analysis we confined ourselves to the hard-collision model because in the speed-independent case, lineshapes obtained on the basis of hard- and soft-collision approaches differ by 0.1% only. From this analysis, the collisional-narrowing coefficients were determined and, therefore, the optical diffusion coefficients were also obtained. We have also considered speed-dependent effects in our data analysis and found that they do not play any important role in our case.

2. LINESHAPES

In this work we have analyzed lineshapes in the hard-collision approximation (*3, 4, 16*). The Nelkin–Ghatak profile (NGP) (*3, 4*) obtained in this approach describes shapes of isolated Doppler and pressure-broadened and shifted lines taking into account the Dicke narrowing. The NGP can be written in the form

$$S(\nu) = \mathrm{Re}\left\{\frac{J(\nu)}{1 - \pi\beta J(\nu)}\right\}, \qquad [1]$$

where

$$J(\nu) = \frac{1}{\pi}\int d^3\mathbf{v}\, f_M(\mathbf{v}) \times \{\gamma_L(\nu) + \beta - i[\nu - \nu_0 - \Delta(\nu) - \mathbf{k}\cdot\mathbf{v}/(2\pi)]\}^{-1}. \qquad [2]$$

Here ν_0 is the unperturbed frequency of the absorbed radiation, $\mathbf{k}$ is the wave vector of the absorbed radiation ($k = 2\pi\nu_0/c$, c is the speed of light), $f_M(\mathbf{v})$ is the Maxwellian distribution of the absorber velocity $\mathbf{v}$, γ_L is the collisional width, and Δ is the collisional shift of the line. The effective frequency of velocity-changing collisions

$$\beta = \frac{k_B T}{2\pi M D} \qquad [3]$$

is dependent on gas temperature T (k_B is the Boltzmann constant) and the diffusion coefficient D of absorber in perturber gas. If the Dicke narrowing can be neglected, that means when $\beta = 0$, the NGP can be reduced to the well-known Voigt profile.

The collisional width γ_L (HWHM), shift Δ, and effective narrowing parameter β are linearly dependent on the perturber pressure p. In addition, the relations between these quantities and the corresponding broadening, shift, and narrowing coefficients (C_b, C_s, and C_n), expressed in megahertz per Torr, are

$$\gamma_l = pC_b \qquad \Delta = pC_s \qquad \beta = pC_n. \qquad [4]$$

3. EXPERIMENTAL DETAILS

Our experimental arrangement used for collision-broadened investigations is schematically shown in Fig. 1. The laser source was a fiber-coupled distributed feedback (DFB) diode laser (Sensor Unlimited, model SU 1393-CF-I-FC), including an optical isolator to prevent spurious optical feedback. It emitted at 1.393 μm at room temperature with a maximum power of about 1 mW while the temperature and current tuning rates were 0.10 nm/°C and 0.0051 nm/mA, respectively. The laser linewidth was about 10 MHz, which resulted in much narrower than molecular absorption widths that in our experimental conditions were typically of several hundreds of megahertz. The laser wavelength was temperature stabilized and driven by a low-noise current supply.

Laser-frequency calibration was performed by recording the transmitted peaks from a 2-GHz free-spectral range confocal Fabry–Perot interferometer.

Before reaching the sample cell, the laser beam was split into two parts by using a $\lambda/2$ plate and a polarized cube. One beam experienced the absorption from the sample, while the second one crossed a reference cell with a residual vacuum of few millitorr. The absorption of water vapor in air was taken into account, making the optical path of the two beams as equal as possible. Using two identical photodiodes and a proper gain balance, the difference between the two signals enabled us to cancel both the effects of water-vapor absorption and amplitude modulations introduced during the laser-frequency scans.

The output signal from the differential amplifier was then sent to a digital oscilloscope and to a personal computer for data acquisition.

The absorption cell was a 1-m-long cylindrical Pyrex tube. To measure the broadening coefficients in presence of N_2 and O_2, we operated at water-vapor pressures lower than 1 Torr to keep the absorbance below 5%. Similarly, for self-broadening measurements, where higher water-vapor pressures were em-

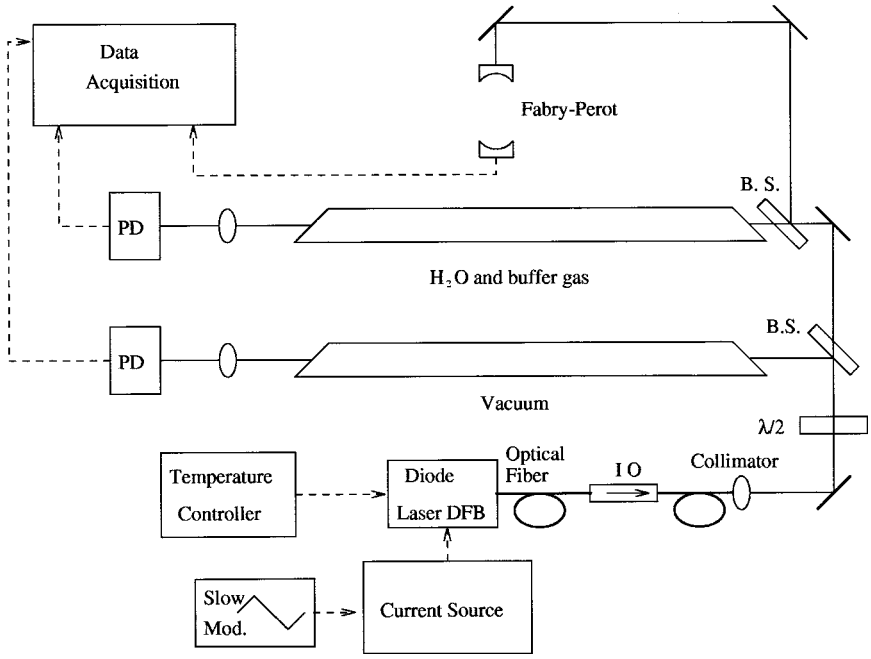

FIG. 1. Scheme of the absorption spectrometer developed for collisional-broadened coefficient measurements. OI stands for the optical isolator, while PD stands for the photodetector.

ployed, a shorter cell (10-cm-long) was used, in order to assume the molecular sample as optically thin. The cells were evacuated with a rotative pump reaching a residual vacuum of 10^{-2} mTorr while nitrogen was fluxed at atmospheric pressure through the cell to reduce the effect of water-vapor adsorption from the cell walls.

4. RESULTS AND DISCUSSION

4.1. Collisional Broadening

The rovibrational lines of the $H_2{}^{16}O$ and $H_2{}^{18}O$ molecules investigated in this work belong to the combination band $\nu_1 + \nu_3$ and to the first overtone $2\nu_1$ band in the 1.39-μm wavelength region. Their assignments were done on the basis of Refs. (*28, 29*) and a complete spectroscopic identification is reported in Table 1. The absorption coefficient of these lines ranges between 1 and 5×10^{-4} cm^{-1} Torr^{-1}. Under our experimental conditions, the gas sample could be assumed as optically thin and the Beer–Lambert law reduces to

$$\frac{I_0(\nu) - I(\nu)}{I_0(\nu)} \approx K(\nu)\, p_{H_2O} L, \qquad [5]$$

where I_0 and I are the incident and transmitted laser intensities, $K(\nu)$ is the absorption cross section (cm^{-1} Torr^{-1}) which is proportional to the function describing lineshape, p_{H_2O} is the water-vapor pressure, and L is the length of the absorption path.

To determine the linewidth γ_L, the recorded spectra were fitted with the standard VP. This profile provided good fits for most of the investigated lines while appreciable deviations from it were observed only for some of the investigated lines that will be discussed later.

Our analysis started with pure water-vapor sample at a pressure of few hundreds of millitorr, where collisions are generally negligible. In these conditions the lineshapes could be fitted by a simple Gaussian curve having a Doppler width (FWHM) of 764(8) MHz in good agreement with the theoretical value $\Delta\nu_D = 760$ MHz (calculated at $T = 300$ K). The Doppler width was then used as a fixed parameter in the nonlinear least-squares procedure concerning spectra affected by collisions.

TABLE 1
List of the Lines of $H_2{}^{16}O$ and $H_2{}^{18}O$ Investigated in This Work

line	~ [cm^{-1}]	$(J\ K_a\ K_c)_{upper}$	$(J\ K_a\ K_c)_{lower}$	vibrational band
		$H_2{}^{16}O$ lines		
N.1	7185.5960	6 6 0	6 6 1	$\nu_1+\nu_3$
N.2	7182.9495	2 1 2	3 1 3	$\nu_1+\nu_3$
N.3	7182.2091	1 0 1	1 1 0	$2\nu_1$
N.4	7181.1557	2 0 2	3 0 3	$\nu_1+\nu_3$
		$H_2{}^{18}O$ lines		
N.5	7184.4561	1 1 1	2 1 2	$\nu_1+\nu_3$
N.6	7183.5871	5 5 1	5 5 0	$\nu_1+\nu_3$
N.7	7182.0937	1 0 1	2 0 2	$\nu_1+\nu_3$

Note. For each line, we indicate the isotope species and give the wavenumber of the transition (cm^{-1}) and the upper and lower state vibrational and rotational assignment of the transition.

The VP was calculated using the Gautschi and Kolbig routine (*30*)

$$w(z) = u(x, y) + i\nu(x, y)$$
$$= \exp(-z^2)\left[1 + \frac{2i}{\sqrt{\pi}}\int_0^z \exp(t^2)dt\right] \quad [6]$$

being

$$z = x + iy = \left[\frac{\nu - \nu_0}{\Delta\nu_D} + i\,\frac{\gamma_L}{\Delta\nu_D}\right]2\sqrt{\ln 2} \quad [7]$$

and the real part of $u(x, y)$ is the well-known convolution integral of the Voigt profile.

The Gautschi and Kolbig routine was available as a routine in the CERN library as well as the nonlinear least-squares procedure (Minuit program). A linear function was added to the Voigt formula to take into account background signals coming from residual amplitude modulation of the laser intensity. In addition, the same formula was multiplied by a second linear function in order to take into account asymmetry caused by laser amplitude variations during the frequency scan since as experimental profile we recorded just the difference between the incident and the transmitted intensity and not the absorbance I/I_0.

The number of experimental points recorded for each spectra was on the order of 500 and the laser frequency scans covered more than three times the linewidth in order to appropriately include the line wings contributions.

The typical fit of the line $1_{01} \rightarrow 1_{10}$ centered at 7182.2091 cm^{-1} (line N.3 of Table 1) is shown in Fig. 2. The water-vapor pressure was 400 mTorr, while the N_2 pressure was 200 Torr. The goodness of fit was checked by monitoring deviations between the experimental points and the calculated ones, expressed as a percentage of the maximum of the VP, is shown in the lower part of Fig. 2. As can be noted, agreement between the experimental and fitted curves is quite good, although the residual is weakly structured (see the next section for a more complete discussion on the latter feature). This kind of analysis was repeated, changing the nitrogen pressure from 50 up to 400 Torr, and a similar study was done when oxygen was used as buffer gas. On the contrary, for the self-broadening study the water-vapor pressure was varied within a narrower range between 1 and 10 Torr to avoid the water-vapor condensation and to keep the absorption below 5%.

A fit with a linear function, performed for each set of data of Fig. 3, provided the broadening coefficient C_b. This analysis was extended to the other lines listed in Table 1 and the measured broadening coefficients are reported in Table 2.

For the $H_2{}^{16}O$ lines investigated in this work, Delaye *et al.* (*31*) have calculated the broadening coefficients on the basis of a theoretical model developed by Robert and Bonamy (*32*) (RB theory). These results are also reported in Table 2. As can be noted, for most of the investigated lines there is satisfactory agreement between our experimental results and the RB theoretical predictions. Nevertheless, some discrepancies, larger than the 3σ, were observed for the line N.1 perturbed by O_2, which also exhibited broadening coefficients smaller than those measured for the other lines. Moreover, appreciable deviations from the standard VP were observed for this line and for the $H_2{}^{18}O$ line N.6. A more detailed analysis of both these lines will be provided in the next paragraph.

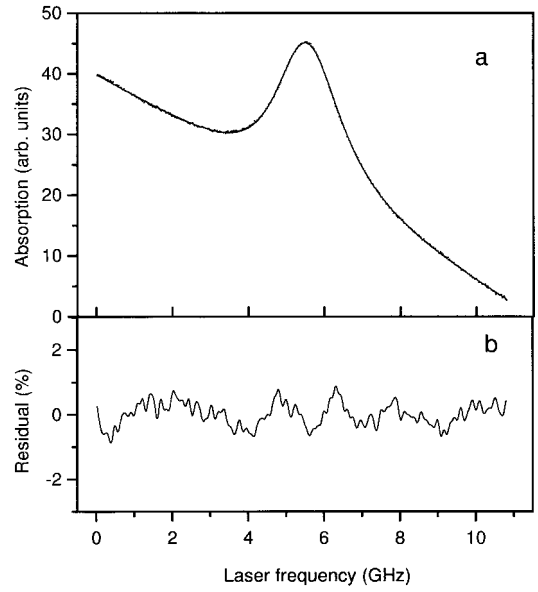

FIG. 2. Comparison between the experimental points and the fitted curve (Voigt profile) for the line $1_{01} \rightarrow 1_{10}$ centered at 7182.2091 cm^{-1} (curve a) at p_{N_2} = 200 Torr and p_{H_2O} = 400 mTorr. Part b shows the residual obtained from the least-squares fitting calculated as explained in the text.

As also found by Gasster *et al.* in Ref. (*33*) for transitions in the microwave region and by Grossman and Browell for the $3\nu_1 + \nu_3$ and $2\nu_1 + \nu_3$ bands (*23, 24*), we observed that the nitrogen perturber was more effective than oxygen. In column five of Table 2, we report the experimental and theoretical ratios between the broadening coefficients for nitrogen and oxygen. Except for the case of lines N.1 and N.6 (which will be discussed later), this ratio varied between 1.57 and 1.72, which differs for less than 10% from the RB estimations. That is also in agreement with the results found by the authors of Ref. (*33*), which found $C_b(N_2)/C_b(O_2) = 1.6(3)$ and those of the Ref. (*24*), which also found $C_b(N_2)/C_b(O_2)$ to vary in the range between 1.65(6) and 1.74(8). Differences in the collisional rate of nitrogen and oxygen are probably due to their different quadrupole moments, Q, which play an important role in the dipole–quadrupole interaction occurring in the collision between H_2O and N_2 or O_2 molecules. Indeed, the quadrupole moment of these molecules is $Q_{N_2} = -3.04 \times 10^{-26}$ esu cm^2

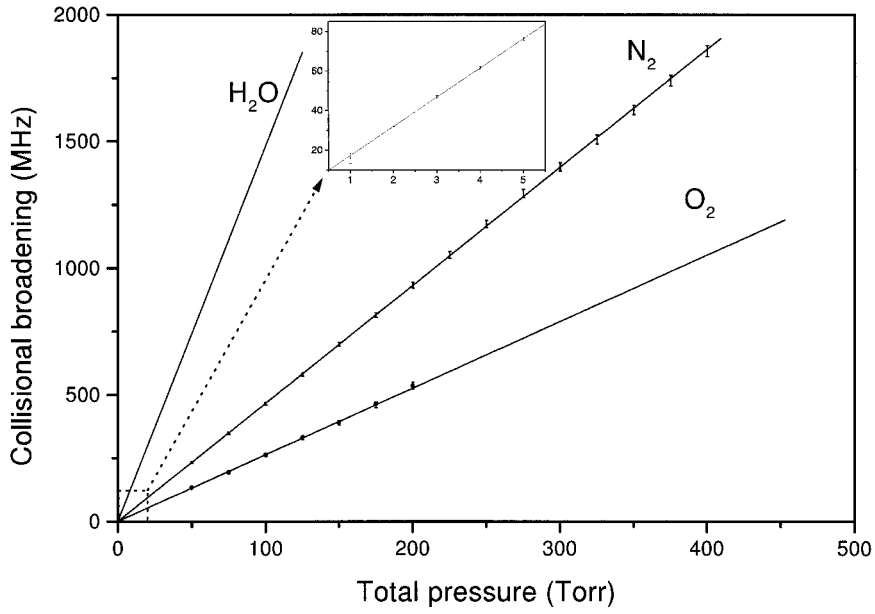

FIG. 3. Experimental behavior of the Lorentzian component γ_L (HWHM) of the $1_{01} \rightarrow 1_{10}$ as a function of the total pressure for different collision partners: pure water vapor, H_2O–N_2, H_2O–O_2, and mixtures. In the insert is reported the self-broadening width in an expanded horizontal scale.

and $Q_{O_2} = -0.78 \times 10^{-26}$ esu cm^2 (*33*), while their ratio, Q_{N_2}/Q_{O_2}, is 3.9. This value, of course, cannot be directly compared with the ratio of the broadening coefficients since the dependence on quadrupole moments occurs in a nontrivial way in the RB theory.

The knowledge of pressure-broadening coefficients of H_2O lines caused by N_2 and O_2 collisions allowed us to estimate also the pressure broadening in presence of air ($a_{air} = 0.79a_{N_2} + 0.21a_{O_2}$). This is of particular interest for detection of water vapor in air using lidar techniques or high-sensitivity spectroscopic-technique detection based on wavelength modulation spectroscopy (WMS), as better discussed in Refs. (*34*, *35*).

Finally, as it can be seen in Table 2, the self-broadening coefficients are larger than the N_2- and O_2-broadening coefficients, which is well understood considering the stronger dipole–dipole interaction which takes place in the self-broadening case.

4.2. Collisional Narrowing

We have found that the lines N.1 and N.6 are not correctly fitted by the standard VP. It can be mainly caused by the Dicke narrowing in our case. Both $H_2{}^{16}O$ lines centered at 7185.5960 cm^{-1}, $J = 6$ (line N.1 of Table 1), and the $H_2{}^{18}O$ line N.6 at 7183.5871 cm^{-1}, $J = 5$, present a broadening coefficient quite smaller than those observed for lines with lower J. It can occur when high-rotational quantum numbers J are involved in the investigated lines since for them the quenching cross sections are usually reduced.

To investigate the Dicke-narrowing effect, the lineshapes of the line N.1 were first fitted using a standard VP but leaving the Doppler width as free parameter. As expected, we found that the Doppler width decreased versus the perturber gas pressure reaching, for instance, a value of about 420 MHz at a perturber pressure $P_{O_2} = 300$ Torr. This result represents an "empirical"

TABLE 2
Measured Collisional Coefficients for Self-, N_2-, and O_2-Broadening Obtained Using a Standard Voigt Profile

line	$C_h(N_2)$ [MHz/Torr]		$C_h(O_2)$ [MHz/Torr]		$C_h(H_2O)$ [MHz/Torr]		$C_h(N_2)/C_h(O_2)$	
	this work	Ref[31]	this work	Ref[31]	this work	Ref[31]	this work	Ref[31]
N.1	1.20(2)	1.68	0.50(1)	1.27	6.3(2)	7.7	2.40(6)	1.32
N.2	3.95(2)	4.17	2.29(2)	2.56	18.3(9)	17.8	1.72(2)	1.63
N.3	4.66(2)	4.60	2.63(3)	3.07	14.78(9)	15.77	1.70(2)	1.50
N.4	4.67(3)	4.30	2.74(11)	2.81	_	_	1.70(7)	1.53
N.5	4.27(1)	_	2.51(3)	_	_	_	1.70(2)	_
N.6	2.26(1)	_	0.99(4)	_	_	_	2.28(9)	_
N.7	4.03(3)	_	2.57(2)	_	_	_	1.57(2)	_

Note. The ratios of N_2- and O_2-broadening coefficients are also reported.

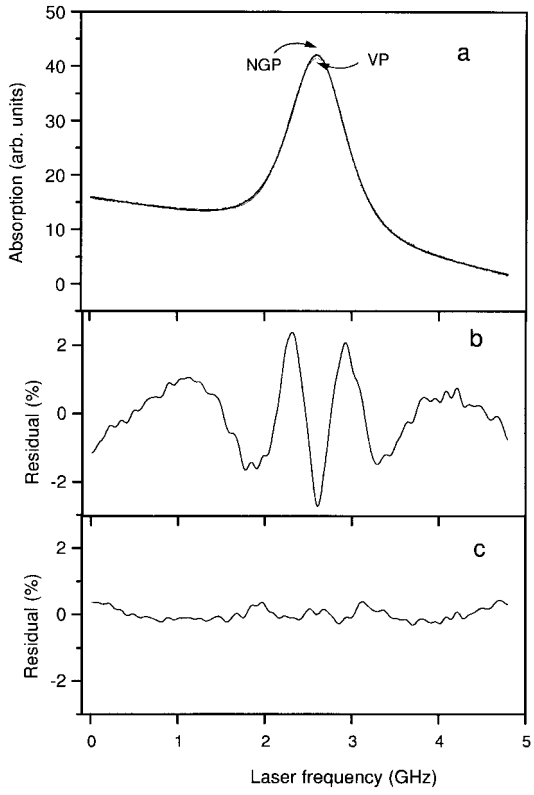

FIG. 4. Results of least-squares fitting to the VP (dashed line) and NGP (continuous line) of the line $6_{60} \rightarrow 6_{61}$ at 7185.5960 cm^{-1} at $p_{O_2} = 175$ Torr (a). The middle trace (b) and lower trace (c) represent the percentage residual from the fitted VP and NGP, respectively.

evidence of Dicke-narrowing effect. Nevertheless, in order to provide a more quantitative analysis of Dicke effect, we took into account the influence of the velocity-changing collisions on the shape of the spectral line described in Section 2. In our analysis we used the NGP to fit our experimental lineshapes. In our numerical procedure the center and the intensity of the line, the Lorentzian width $\gamma = C_b^{\cdot} p$ and the narrowing parameter $\beta = C_n^{\cdot} p$ were free parameters, while the Doppler width was fixed. A comparison between the experimental spectrum and the fitted VP and NGP is shown in Fig. 4 for the line N.1 at $P_{O_2} = 175$ Torr. In addition, the middle trace and the lower trace of Fig. 4 represent the percentage deviations between the measured lineshape and the fitted VP and NGP, respectively. In particular, deviations from VP are similar to those shown by Varghese and Hanson (*36*), obtained as a result of a fit of a numerically generated Dicke-narrowing profile with a VP. Anyway, comparing the residual of part (b) and (c) of Fig. 4, it can be seen that the NGP fits our experimental profile very well. This analysis was repeated by changing the O_2 and N_2 pressures in the range between 50 and 500 Torr for both the lines N.1 and N.6. The values found for γ and β provided a linear behavior when plotted against the total pressure for both N_2 and O_2 perturbers (Fig. 5 refers to the case of line N.1). From a linear fit of the γ behaviors, we found the following new values for the broadening coefficients $C_b(N_2)$ and $C_b(O_2)$:

$$\begin{aligned} \text{line N.1} \quad & C_b(N_2) = 1.91(1)\ \text{MHz/Torr} \\ & C_b(O_2) = 1.12(1)\ \text{MHz/Torr} \\ \text{line N.6} \quad & C_b(N_2) = 2.38(1)\ \text{MHz/Torr} \\ & C_b(O_2) = 1.24(1)\ \text{MHz/Torr.} \end{aligned} \qquad [8]$$

In particular, for the line N.1 the revisited broadening coefficients obtained from the NGP analysis show better agreement with the RB values. Indeed, now the discrepancies between theoretical and experimental values are on the order of 10%, while those found from the VP analysis resulted also one order of magnitude larger (see Table 2). On the contrary, for smaller differences found between the VP and NGP analysis for the line N.6, unfortunately, no theoretical data are available.

The line N.1 was also revisited using NGP for the self-broadening case and the new broadening coefficient was $C_b(H_2O) = 7.5(2)$ MHz/Torr against 6.3(2) MHz/Torr obtained with the VP analysis. Again the NGP result is in better agreement with the theoretical value of 7.7 MHz/Torr.

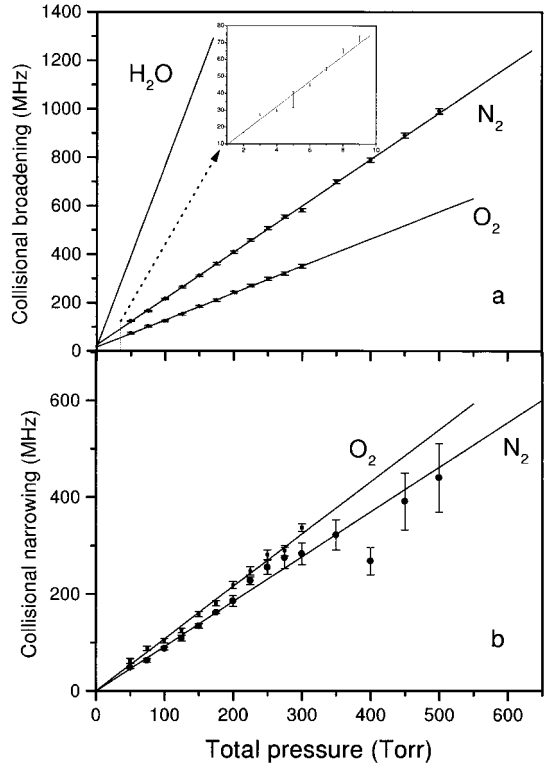

FIG. 5. Experimental behaviors of the effective frequencies of broadening collision f_b and narrowing collisions f_n of the line $6_{60} \rightarrow 6_{61}$ as a function of the total pressure obtained from NGP analysis. In the insert is reported the self-broadening width in an expanded horizontal scale.

TABLE 3
Measured Collisional Narrowing Coefficient C_n and Diffusion Coefficients D Calculated at $p = 1$ atm, in Various Buffer Gases

line	buffer gas	C_n [MHz/Torr]	D [cm^2/s]	D_{mass} [cm^2/s]	$(D-D_{mass})/D$
N.1	N_2	0.93(3)	0.312(10)	0.288	8%
	O_2	1.08(4)	0.269(10)	0.296	9%
N.6	N_2	0.81(4)	0.322(10)	0.279	13%
	O_2	0.58(3)	0.451(11)	0.286	37%

A similar analysis was also done for the linear behavior concerning the collisional-narrowing parameter β plotted for the line N.1 in part (b) of Fig. 5. In particular, the slope of the straight line of Fig. 5b provided the β_{diff} parameter and, on the basis of Eq. [3], also the optical diffusion coefficient D which is listed in Table 3 for the two analyzed lines. In the same table are also reported the values of the mass diffusion coefficient D_{mass} obtained from the diffusion theory (*37, 38*)

$$D_{mass} = 0.00262\epsilon_{12}\frac{\sqrt{\frac{T^3}{2\mu}}}{Tp\Omega_{12}\sigma_{12}}, \qquad [9]$$

where μ is the reduced mass of the absorber–perturber system, ϵ_{12} and σ_{12} are the Lennard–Jones parameters (*20, 39*) concerning the dipole–quadrupole interaction, Ω is a tabulated factor which takes into account the dynamic of the collision, and p is the perturber pressure (the diffusion coefficients of Table 3 were calculated at $p = 1$ atm). As can be seen from Table 3, the agreement between D and D_{mass} is quite good except for the line N.6 investigated in H_2O–O_2 mixtures. The disagreement between optical and mass diffusion coefficients of H_2O in O_2 observed for the line N.6 could be caused by the correlation between velocity-changing and dephasing collisions.

For the systems considered in this work, H_2O–N_2 and H_2O–O_2, the α coefficient, the ratio of perturber and absorber masses, is equal to 1.6 and 1.8, respectively. For such values of α, one could expect that speed-dependent effects play some role in the case of investigated lines. To explain it, the lineshapes were analyzed including the speed-dependent effect by using the SDNGP introduced in Section 2. However, the results of this kind of analysis applied to the line N.1 and N.6 provided no appreciable differences with respect to the NGP. This means that it is necessary to assume collisional width and shift are speed-independent or weakly dependent on the absorber speed. Therefore we can say that the influence of the speed-dependent effects on shapes of investigated lines is much smaller then the influence of the Dicke narrowing.

Finally, the NGP analysis was also extended to the other lines having low J values but the new estimated broadening coefficients resulted statistically consistent with those already found from VP analysis.

5. CONCLUSIONS

Lineshapes analysis of H_2O transitions in the 1.39-mm wavelength region was performed to study the self-broadening and the broadening induced by nitrogen and oxygen. A standard Voigt profile was successfully used to measure the broadening coefficients for most of the investigated lines. Good agreement was also found between our experimental results and the theoretical predictions based on the Robert and Bonamy theory. Nevertheless, we have found the Dicke-narrowing effect for some transitions, involving relatively high rotational quantum numbers J, of which collisional broadening coefficients were smaller than coefficients of other investigated lines. For these lines the Voigt profile proved inadequate and the Nelkin–Ghatak profile was instead used to fit the experimental spectra. The revisited broadening coefficients estimated from the NGP analysis provided better agreement with the RB theory. Moreover, from the analysis of the effective velocity-changing collision frequency, the optical diffusion coefficients were also found. Most of these coefficients agree with calculated mass diffusion coefficients. On the contrary, the analysis based on NGP for lines involving low J values provided negligible difference in the broadening coefficients determined from VP fits.

The results reported in this work can help for a better understanding of the collisional physics of the H_2O molecule but can also provide useful data for many applications concerning the study of this molecule in the atmosphere.

Nevertheless, on the basis of the found results, further investigations could be interesting for testing the adequacy of the different profiles contemplated within the velocity-changing collisional models. For instance, a systematic analysis versus the rotational number J could be done by investigating a richer set of lines belonging to the vibrational bands here investigated using a more tunable laser source. Moreover, the choice of perturbers having a mass varying over a wider range or exhibiting different kinds of interactions with H_2O molecules could also be useful to better explore the soft- and hard-collision regimes and speed-dependent effects.

ACKNOWLEDGMENTS

The authors are grateful to Prof. A. Bielski for a fruitful discussion and to Dr. R. S. Trawinski for a critical reading of the manuscript.

REFERENCES

1. R. H. Dicke, *Phys. Rev.* **89,** 472–473 (1953).
2. L. Galatry, *Phys. Rev.* **122,** 1218–1223 (1961).
3. M. Nelkin and A. Ghatak, *Phys. Rev. A: Gen. Phys.* **135,** 4–A9 (1964).
4. S. G. Rautian and I. I. Sobelman, *Sov. Phys. Usp.* **9,** 701–716 (1967).
5. P. R. Berman, *J. Quant. Spectrosc. Radiat. Transfer* **12,** 1331–1342 (1972).
6. J. Ward, J. Cooper, and E. W. Smith, *J. Quant. Spectrosc. Radiat. Transfer* **14,** 555–590 (1974).
7. H. M. Pickett, *J. Chem. Phys.* **73,** 6090–6094 (1980).
8. E. L. Lewis, "Spectral Line Shapes" (J. Szudy, Ed.), Vol. 5, p. 485, Ossolineum Publ., Wroclaw, 1988; M. Harris, E. L. Lewis, D. McHugh, and I. Shannon, *J. Phys. B: At., Mol. Opt. Phys.* **17,** L661–667 (1984); *J. Phys. B: At., Mol. Opt. Phys.* **19,** 3207–3211 (1986); I. Shannon, M. Harris, D. McHugh, and E. L. Lewis, *J. Phys. B: At., Mol. Opt. Phys.* **19,** 1409–1424 (1986).
9. R. L. Farrow, L. A. Rahn, G. O. Sitz, and G. J. Rosasco, *Phys. Rev. Lett.* **63,** 746–749 (1989).
10. D. Robert, J. M. Thuet, J. Bonamy, and S. Temkin, *Phys. Rev. A: Gen. Phys.* **47,** R771–773 (1993).
11. S. Brym, R. Ciurylo, R. S. Trawinski, and A. Bielski, *Phys. Rev. A: Gen. Phys.* **56,** 4501–4507 (1997); A. Bielski, S. Brym, R. Ciurylo, and J. Szudy, *Eur. Phys. J.* **D8,** 177–187 (2000).
12. P. Duggan, P. M. Sinclair, A. D. May, and J. R. Drummond, *Phys. Rev. A: Gen. Phys.* **51,** 218–224 (1995).
13. R. Ciurylo and J. Szudy, *J. Quant. Spectrosc. Radiat. Transfer* **57,** 411–423 (1997).
14. B. Lance, G. Blanquet, J. Walrand, and J. P. Bouanich, *J. Mol. Spectrosc.* **185,** 262–271 (1997).
15. P. Duggan, P. M. Sinclair, R. Berman, A. D. May, and J. R. Drummond, *J. Mol. Spectrosc.* **186,** 90–98 (1997).
16. R. Ciurylo, *Phys. Rev. A: Gen. Phys.* **58,** 1029–1039 (1998).
17. B. Lance and D. Robert, *J. Chem. Phys.* **109,** 8283–8289 (1998).
18. F. Chaussard, X. Michaut, R. Saint-Loup, H. Berger, P. Joubert, B. Lance, J. Bonamy, and D. Robert, *J. Chem. Phys.* **112,** 158–166 (2000).
19. A. S. Pine, *J. Quant. Spectrosc. Radiat. Transfer* **62,** 397–423 (1999).
20. R. Ciurylo, A. S. Pine, and J. Szudy, *J. Quant. Spectrosc. Radiat. Transfer* **68,** 257–271 (2000).
21. D. Priem, F. Rohart, J. M. Colmont, G. Wlodarczak, and J. P. Bouanich, *J. Mol. Struct.* **517,** 435–454 (2000).
22. R. S. Eng, A. R. Calawa, T. C. Harman, P. L. Kelley, and A. Javan, *Appl. Phys. Lett.* **21,** 303–305 (1972).
23. B. E. Grossmann and E. V. Browell, *J. Mol. Spectrosc.* **136,** 264–294 (1989).
24. B. E. Grossmann and E. V. Browell, *J. Mol. Spectrosc.* **138,** 562–595 (1989).
25. V. G. Avetison, A. I. Nadezhdinskji, A. N. Khusnutdinov, P. M. Omarova, and M. V. Zyrianov, *J. Mol. Spectrosc.* **160,** 326–334 (1993).
26. A. S. Pine, *J. Chem. Phys.* **101,** 3444–3452 (1994).
27. P. Joubert, J. Bonamy, D. Robert, J. L. Domenech, and D. Bermejo, *J. Quant. Spectrosc. Radiat. Transfer* **61,** 519–531 (1999).
28. R. A. Toth, *Appl. Opt.* **33,** 4851–4867 (1994).
29. R. A. Toth, *Appl. Opt.* **33,** 4868–4879 (1994).
30. J. Humlicek, *J. Quant. Spectrosc. Radiat. Transfer* **21,** 309–313 (1979); *J. Quant. Spectrosc. Radiat. Transfer* **27,** 437–444 (1979).
31. C. Delaye, J. M. Hartmann, and J. Taine, *Appl. Opt.* **28,** 5080–5087 (1989).
32. D. Robert and J. Bonamy, *J. Phys. (Paris)* **40,** 923–943 (1979).
33. S. D. Gasster, C. H. Townes, D. Goorvitch, and F. D. Valero, *J. Opt. Soc. Am. B: Opt. Phys.* **5,** 593–601 (1988).
34. L. Gianfrani, G. Gagliardi, G. Pesce, and A. Sasso, *Appl. Phys. B* **64,** 487–491 (1997).
35. L. Gianfrani, M. R. Santovito, and A. Sasso, *J. Mol. Spectrosc.* **186,** 207–212 (1997).
36. P. L. Varghese and R. K. Hanson, *Appl. Opt.* **23,** 2376–2385 (1984).
37. S. Chandrasekhar, *Rev. Mod. Phys.* **15,** 1–89 (1943).
38. J. O. Hirschfelder, *in* "Molecular Theory of Gases and Liquids," Wiley, New York, 1954.
39. B. Labani, *J. Chem. Phys.* **87,** 2781–2789 (1987).